RoACH: An autonomous 2.4g crawling hexapod robot

Aaron M. Hoover, Erik Steltz, Ronald S. Fearing
University of California, Berkeley, CA 94720 USA
{ahoover, ees132, ronf}@eecs.berkeley.edu

***Abstract*— This work presents the design, fabrication, and testing of a novel hexapedal walking millirobot using only two actuators. Fabricated from S2-Glass reinforced composites and flexible polymer hinges using the smart composite microstructures (SCM) process, the robot is capable of speeds up to 1 body length/sec or approximately 3cm/s. All power and control electronics are onboard and remote commands are enabled by an IrDA link. Actuation is provided by shape memory alloy wire. At 2.4g including control electronics and battery, RoACH is the smallest and lightest autonomous legged robot produced to date.**

I. INTRODUCTION

Legged vehicles offer some significant advantages over their wheeled counterparts: they can traverse rough terrain with obstacles as high or higher than the height of their hips [11][9], they are not necessarily non-holonomically constrained [10], and they enable extreme abilities like climbing vertical surfaces [8]. In addition to those attributes, legged robots and animals alike have been shown to be capable of achieving open loop dynamic stability through the tuning of mechanical system parameters like spring and damping constants [7].

Very small robots with micron scale features and millimeter scale components (millirobots) also provide advantages over larger robots: their small size enables them to operate in environments where large robots would be impractical or impossible; their low cost allows them to be produced in large quantities, and large numbers of them can be networked to form highly mobile and robust sensor and communication networks.

In this work, we merge the areas of legged locomotion and millirobotics to present a 2.4g robotic, autonomous, crawling hexapod (RoACH) capable of sustained locomotion. The robot makes use of a process called smart composite microstructures (SCM) [12] in which rigid composite links and flexible polymer hinges are fabricated in an integrated fashion. The flat structure that results is folded to produce functional articulated mechanisms which are then combined to form the skeleton of the robot.

To provide necessary background as well as lay the foundation to support our design decisions, we first provide a brief overview of the SCM process. We follow this overview by introducing the mechanical design of the robot, including the kinematics as well as static force considerations and actuator specifications. We then present the power, control, and communication electronics design. Finally, we conclude with discussion of the robot's performance in a series of experimental trials.

This work represents the first step in applying the enabling technology of SCM to produce a fully functional, integrated, legged millirobot. As such, we stress the importance of the robot's mechanical design, the use of the SCM process, and the integration of the actuation, power, and control, but we do not present a dynamic system model, a map of control inputs to outputs, or energy/efficiency analysis. While we recognize the necessity and importance of these tools, the contribution of this work is proving the viability of legged machines at the milliscale through the integration of novel processes and technologies.

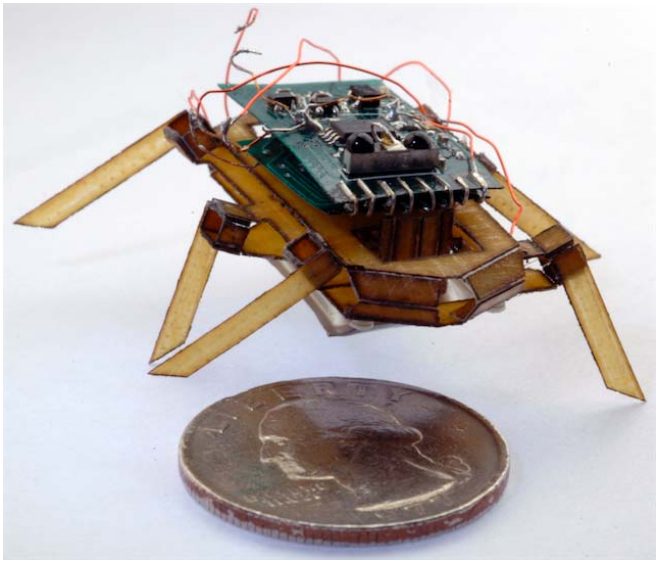

Fig. 1. The 2.4g RoACH standing over a US quarter

II. FABRICATION PROCESS

SCM is a process which integrates laser micromachined composite fiber laminates with polymer films to create mechanisms consisting of rigid composite links and compliant polymer hinges as shown in Fig. 3. The process as it is implemented for the fabrication of RoACH is depicted in Fig. 2 and the steps are outlined below.

1) The process begins with a sheet of uncured, pre-impregnated composite fiber laminate (S2-Glass in our case).
2) Gaps are laser micro-machined into the composite fiber using a 25W CO_2 laser (Versalaser, Universal Laser

Systems).

3) A polymer film (PET) is placed on top of the laminate.
4) A laminate with the mirrored cut pattern is placed on top of the polymer layer.
5) The entire structure is cured.
6) The resulting flat structure is released.

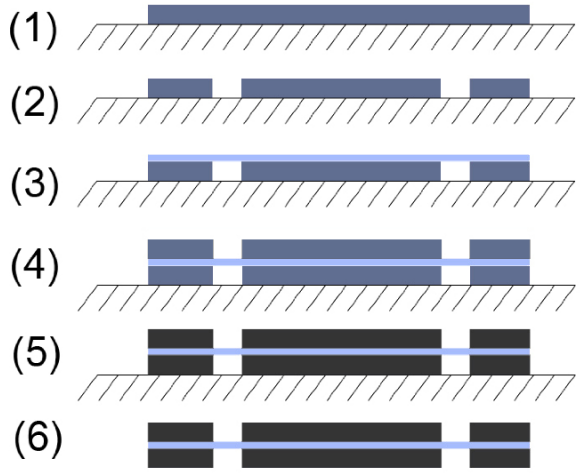

Fig. 2. A step-by-step illustration of the SCM link and hinge fabrication process.

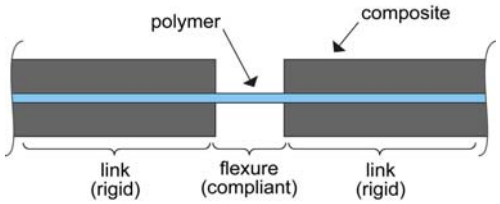

Fig. 3. An SCM flexural hinge made from thin polymer film and rigid composite links [12]

A palette of parts for the construction of RoACH is shown in Fig. 4. This palette demonstrates two distinct advantages of the SCM process. 1) It enables the fabrication of a robot with a large number of articulated joints for the same cost as a robot with a minimal number of joints. For example, RoACH's design uses 57 joints. This is in contrast to robotic design with conventional materials and mechanisms in which the cost of each joint is significant. 2) Multiple copies of parts can be fabricated in parallel. The number of parts that can be made in parallel is limited only by the equipment used to produce them (ie. size of the laser cutting table, volume of the curing oven, etc.). These two factors combined make the fabrication of millirobots very inexpensive in terms of both time and materials. From start to finish (excluding cure time and time required to populate the circuit board), RoACH

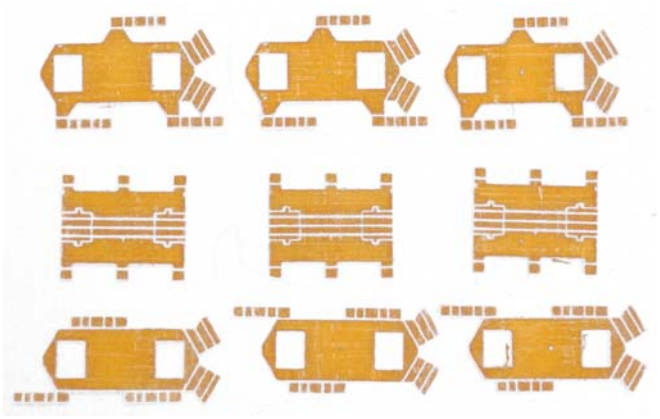

Fig. 4. A palette of flat SCM parts showing 3 complete RoACH thoraxes ready for folding and assembly

requires approximately 8 hours to layup, cut out, assemble, and wire.

The final advantage of the SCM process is that it enables straightforward integration of a variety of actuators which include piezoelectric bending members [13] and, in our case, shape memory alloy wires. Laser micromachining enables exact placement of features to assist in routing and guiding wires or aligning and laminating piezoelectric materials.

However, SCM is not without disadvantages as well. Flexural hinges provide only limited motion - continuous rotations are not possible, and care must be taken to ensure that angular displacements do not exceed elastic strain limits of the material. In addition, off-axis loading conditions such as lateral or buckling loads must be considered and minimized during the design process. Finally, though the final product is a folded 3D articulated structure, the design representation appropriate for fabrication is 2 dimensional. The conceptual difficulty of envisioning 3D designs and realizing them in a flat drawing is significant. Design tools that automate or assist in this process represent an area of research where improvements are needed in order to enable wider adoption of SCM.

III. MECHANICAL DESIGN

Designing millirobots presents unique challenges that result from size constraints. Firstly, as size decreases, surface forces begin to dominate inertial forces as a result of the increase in the surface area to volume ratio. One example of this is the dominant effect of friction at the small scale. Avoiding the effects of friction motivates our choice of the SCM technology which relies on elastic deformation of compliant hinges to provide articulation. SCM has the added advantage of being a near-monolithic fabrication process in which the cost of adding a single joint (and, hence, mechanism complexity) is essentially negligible.

Secondly, size limitations severely affect the power and control electronics budgets. At the milliscale, actuators can be expensive from a weight perspective (in the case of

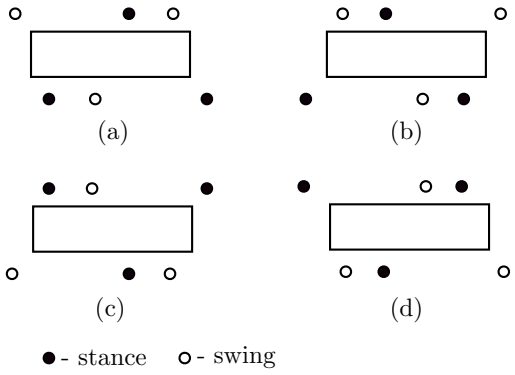

Fig. 5. Diagram of RoACH's alternating tripod gait at four extreme positions

piezoelectric materials) or a power perspective (as is the case with SMA). Thus, minimal actuation becomes a core guiding principle of robotic design at this scale. This minimal actuation constraint necessarily requires "programming" some of the robot's gait into the structure via the kinematics.

Position	Actuator 1	Actuator 2
a	OFF	OFF
b	ON	OFF
c	ON	ON
d	OFF	ON

TABLE I

MAP OF ACTUATOR STATES TO GAIT POSITIONS SHOWN IN FIG. 5

A. Actuation

Given constraints of working at the milliscale, SMA wire was chosen to provide actuation for a number of reasons. Firstly, SMA integrates very nicely with the SCM process. Alignment and routing features can be directly machined into the composites to enable easy attachment and tensioning of the SMA wire. Secondly, SMA wire provides a force in a single direction. One difficulty of working with compliant mechanisms is their susceptibility to off-axis forces and undesirable moments. The single line force between points of attachment of SMA enables greater design freedom. Also, the target speed range (1 - 15Hz) makes SMA viable (we have experimentally measured the bandwidth of 25μm SMA wire to be approximately 7.5 Hz). Lastly, it's incredibly lightweight, making it very power dense.

However, because SMA is a tensile actuator only, it is necessary to provide a return force either with an antagonistic SMA or spring. With SCM, it is possible to design return springs into the hinges of the mechanism. Similar to tendons in animal muscles [3], this approach enables storage of elastic energy which is then returned when the actuator is switched off and the joint returns to its equilibrium state. The characteristics of the SMA actuators for our actuation conditions are summarized in Table III. The SMA wire used in RoACH was 37.5 μm wire (Flexinol, Dynalloy Inc.), and it was attached to the robot by first crimping steel hypo-tubing to the ends and gluing the crimps to the robot's body.

The use of SMA is, however, not without its disadvantages. Lifetime of the wires can be significantly shortened by accidental overstraining or overheating. In our design we have taken care to ensure that preloading of the SMA does not exceed strain limits specified by the manufacturer [1]. In section IV we describe a drive scheme designed to heat the actuator quickly, but avoid overheating so as to ensure the longest life possible. While manufacturer's specifications claim lifetimes on the order of 10^6 cycles, for our configuration, a lifetime on the order of 10^4 - 10^5 cycles is a more reasonable estimate.

B. Kinematics

Given the aforementioned size and power constraints and the choice of SMA wire actuator, RoACH was designed to achieve an alternating tripod gait using two linear actuators. Unlike traditional linkages which use pin joints capable of infinite rotation, flexure-based linkages cannot produce a closed trajectory from a single degree of freedom. Therefore, in order to achieve a closed trajectory for the foot of the robot to follow, it was necessary to use two actuators. RoACH's alternating tripod gait is achieved through a combination of kinematics and basic feedforward, clock-based control. A schematic depiction of the gait and a map of the actuator inputs corresponding to the gait positions are shown in Fig. 5 and Table I respectively.

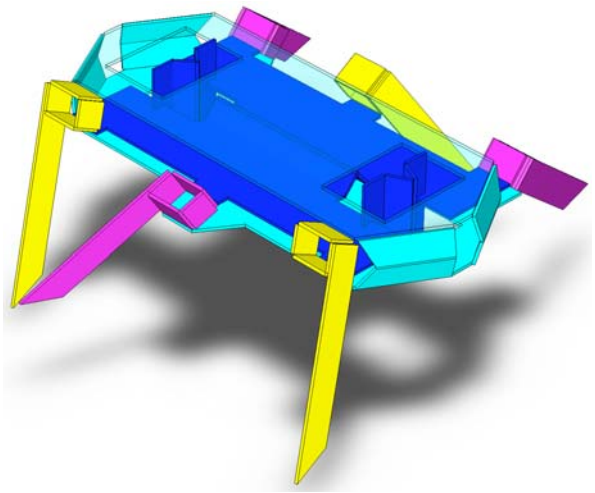

Fig. 6. A CAD model of the robot. The top plate is shown nearly transparent so the inside of the robot may be seen.

RoACH's kinematics can be reduced to two translational degrees of freedom which are appropriately coupled through a central element to fourbar linkages that map those translational inputs into angular outputs. The design is ground-free in the sense that any rigid link could be used to establish the body coordinate system. RoACH's kinematics can be understood by examining two structures and their interactions: the central plate (shown in blue in the CAD

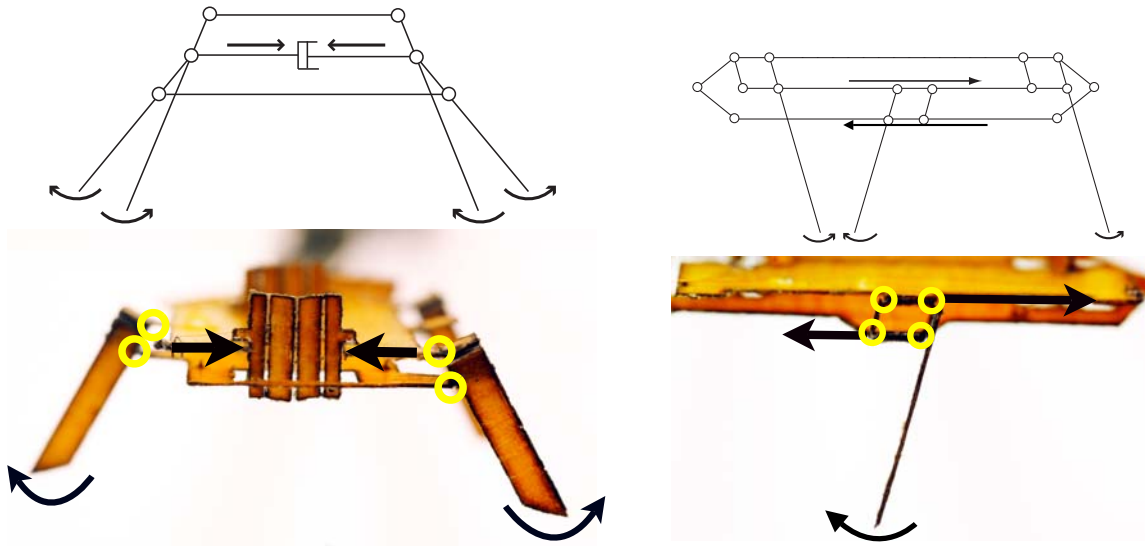

(a) First degree of freedom - into and away from body leg rotation (rear view): model and actual robot (with only one tripod attached)

(b) Second degree of freedom - forward and back leg rotation (side view): model and actual robot (one hip only)

Fig. 7. Crawler kinematics depicting two independent degrees of freedom

model in Fig. 6) and the two outer plates of the body (shown in cyan, with the top plate transparent in Fig. 6). The outer plates are constrained to move together in the horizontal plane, but are free to translate vertically with respect to each other. The middle plate is designed to contract laterally in the horizontal plane and is coupled to the upper and lower plates through fourbar linkages at the "hips" of the robot. From Fig. 6, when the central plate is moved forward along the long axis of the body with respect the outer plates, the magenta tripod swings back and the yellow tripod forward. When the central plate is contracted along the lateral axis of the body the magenta legs are lifted, and the yellow legs are lowered. These motions are also depicted individually in Fig. 7 while Fig. 8 shows the configuration of the SMA wire actuators used to control the two degrees of freedom.

C. Flexure linkage design

Each degree of freedom in the robot begins its actuation cycle at one extreme of its output motion and must be returned to this position at the end of one actuation cycle. A common approach to the this bidirectional motion is to use two SMA actuators in an antagonistic configuration. However, to improve efficiency and simplify actuation, we have chosen to use the flexure hinges as return springs.

Using the short flexure approximation [6], the expression for the angular spring constant of a simple flexure hinge is:

$$K_\theta = \frac{Ebh^3}{L} \tag{1}$$

In Eqn. 1 E is the flexural modulus, b is the width of the flexure, h is the thickness, and L is the length.

The first return spring works in opposition to contraction of the middle plate shown at the top of Fig. 8. It consists

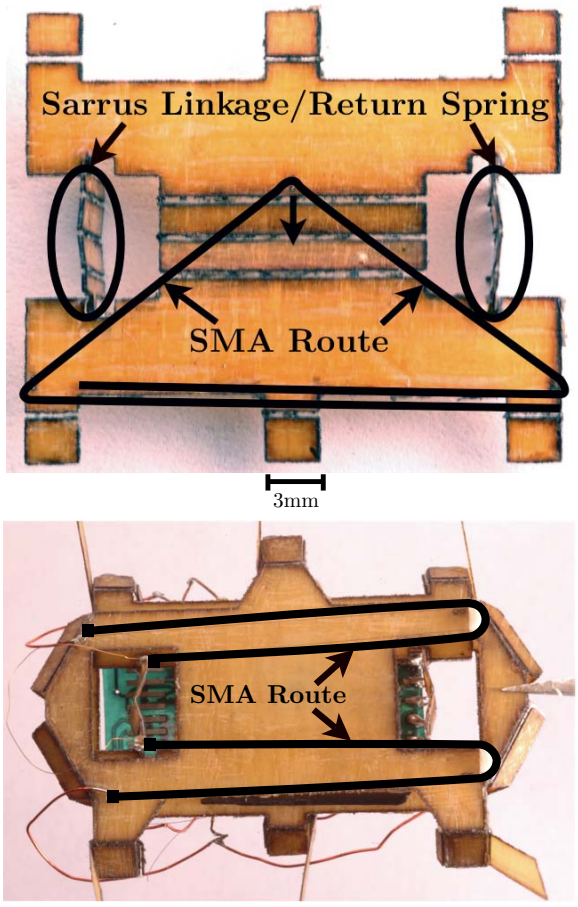

Fig. 8. **Above:** The central contracting plate showing the route for the actuator responsible for lateral raising and lowering of the legs. **Below:** The bottom plate depicting the routing of the actuator connecting the bottom and middle plates and used to control fore-aft swinging of the legs.

of a flexure hinge approximation of a Sarrus linkage - a spatial linkage which provides a single translational degree of freedom. The second degree of freedom is provided by the parallel fourbar linkage at the hip joint shown in Fig **??**. The equivalent spring "constant" (the spring force is a nonlinear function of linkage displacement) for these linkages can be determined using energy methods as follows:

$$\frac{\partial U}{\partial q_1} = \mathbf{F}\frac{\partial s}{\partial q_1} = \mathbf{F}\frac{\partial s}{\partial x}\frac{\partial x}{\partial q_1} \tag{2}$$

In Eqn. 2 U is the potential or strain energy stored in the linkage, q_1 is a generalized coordinate (angular displacement of a link in our case), s is a generalized output displacement, and x is a linear output displacement. In our case, s and x are equivalent, so we solve for $\mathbf{F}$ as a function of x and differentiate to give the expression for the equivalent linkage spring constant, k:

$$K = \frac{\partial^2 U}{\partial x^2} \tag{3}$$

The full expressions for the spring constants for the Sarrus and fourbar linkages resulting from Eqn. 3 are quite long, so they have not been included here.

In the fourbar linkage it is also possible to induce the linkage to rest in a biased position such that the joint angles are not all 90°. This is accomplished by stiffening the flexure hinges at opposite corners. For a parallel fourbar with 2 joints catercorner from each other having a stiffness, k_1, and the other two having stiffness k_2 the rest angle, θ is given as:

$$\theta = \frac{\pi}{1 + \frac{k_2}{k_1}} \tag{4}$$

Thus it is possible to affect an arbitrary bias angle and therefore set the return point of the leg for the beginning of its stance phase.

IV. ELECTRONICS DESIGN

For very small robots, integration of power and control electronics is a crucial design consideration. Since the selection of lightweight batteries at this scale is limited, the battery represents a high percentage of the overall robot weight. Likewise, since custom integrated circuits are quite expensive, lightweight PC board construction is the most practical solution for electronics design. However, it is still relatively heavy and also represents a significant portion of the robot weight. Therefore, careful selection and design of these components can decrease overall robot weight significantly, improving performance.

A. Control Board

A lightweight control board is needed for driving the SMA actuators as well as for steering, communication, and sensing behaviors. A custom 440mg control electronics board (shown in Fig. 10) was manufactured using, 25 μm core FR4 fiberglass. The board utilizes surface mount components

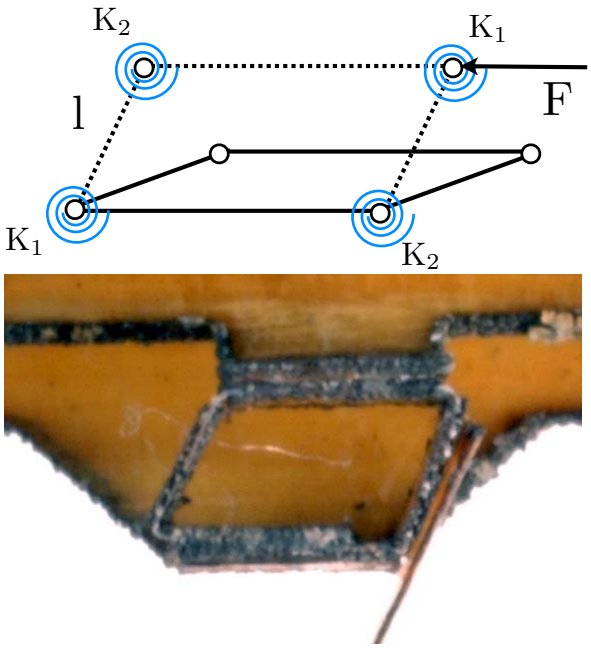

Fig. 9. Above: A model of a biased parallel fourbar (shown relaxed and displaced) using flexure hinges as springs with different rotational spring constants. Below: an actual hip fourbar in equilibrium position on the robot showing the biased return spring for forward and backward swinging of the legs.

System	Component	Mass
Control Electronics 402mg	Blank Board	180mg
	PIC Processor + LEDs	97mg
	Regulator + Battery Monitor	22mg
	IrDA	103mg
SMA Power Electronics 287mg	Blank Board	124mg
	DC-DC Converter	153mg
	Drive Transistors	10mg
Power Supply	Battery	847mg
Structure	Skeleton + Joints	700mg
Actuators	SMA Wires + Crimps	1mg
Wiring	Wiring, Solder, Trim	160mg

TABLE II
MASS BREAKDOWN FOR THE ENTIRE ROBOT

and features a connector not only to the power electronics but also to a sensing "daughter" card. None is presented here but several daughter cards exist for such sensors as accelerometers, gyros, or a compass. This control board is more recent revision of the control board used in [14] that demonstrated autonomous glider navigation toward a light using an infrared sensor.

1) Power and Processing: The control board contains a 10Mips PIC LF2520 processor running at 3.3V through a ZXCL330 low dropout regulator. The PIC processor was chosen for its internal oscillator to save weight and for its low power consumption. Red and green LEDs indicate battery voltage status using a MN1382 battery monitor. RoACH is powered by a 20mAh Lithium polymer battery (Model 301218HS20C, FULLRIVER Battery New Technology Co.)

weighing 850mg (after trimming).

2) Wireless Communication: The board contains a complete implementation of the bidirectional IrDA infrared communication standard common in PDAs and laptops. Infrared communication uses very little power compared with RF technologies like bluetooth. The lack of antenna also decreases the weight of the module. Communication uses the PIC's hardware UART and communicates with a PC at 115.2kbps via a serial port and IrDA converter.

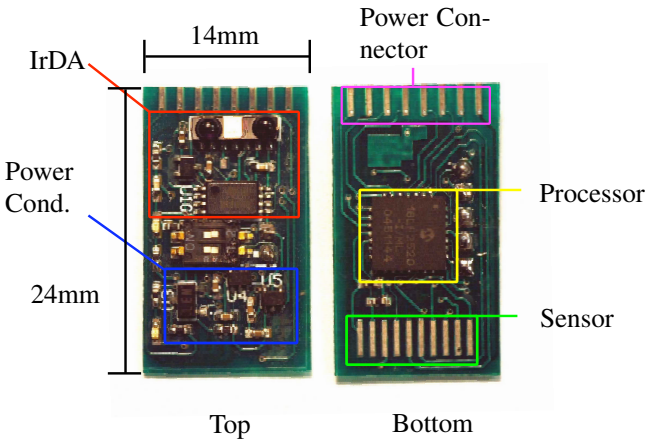

Fig. 10. Top and bottom of the control electronics PC board.

B. SMA Power Supply

SMA wire is a thermal actuator, actuated by resistive heating. Therefore, the power requirement for each actuator is simply given by $P = I^2R$, where R is the resistance of the Flexinol (SMA) wire. The SMA power supply should be capable of driving a variety of wire sizes. Available Flexinol wire diameters and the associated resistance per unit length (from www.dynalloy.com) are shown in Table III.

Wire Diameter (mil)	Force Output (g)	Resistance per Length (Ω/in)	Maximum Pulse Current (mA)
1.0	7	45	60
1.5	17	21	100

TABLE III

TWO FLEXINOL SIZES AND ASSOCIATED CHARACTERISTICS. MAXIMUM PULSE CURRENT ESTIMATES ARE FROM OUR OWN EXPERIMENTS.

The maximum length of SMA wire in the design is approximately 100mm. For 25 μm wire, the resistance is 177 Ω. To drive the maximum of 60mA pulsed current through this resistance, a voltage of 10.6V is needed, meaning a DC to DC converter is necessary to boost from the nominal battery voltage of 3.7V. A safety factor was included to make the target output voltage of the SMA power converter 13.6V. This is the highest voltage necessary to drive either of the wire diameters in Table III. Maximum output power of the proposed DC to DC converter is 0.83W for a single channel driving the 37 μm wire or 1.66W for both channels. This target power output is an upper design bound only; in reality the robot does not have 200mm of Flexinol and both actuators are not pulsed to their maximum drive current at the same time.

A standard boost converter topology was chosen as the DC to DC converter. A Coilcraft LPS4018 15.3μH surface mount inductor weighing 97mg was used for its light weight and high current tolerance (0.86A, 10% drop). Switching is realized via an LT3580 boost converter IC capable of switching frequencies from 200kHz to 2.5MHz. A high speed, high power schottky diode was used for switching (UPS120). Resistors govern both the switching frequency and the output voltage, making the circuit easily customizable for different SMA wire diameters. An efficiency plot for 1MHz and 2MHz switching frequencies at 13.6V output voltage and 3.5V input voltage is shown in Fig. 11.

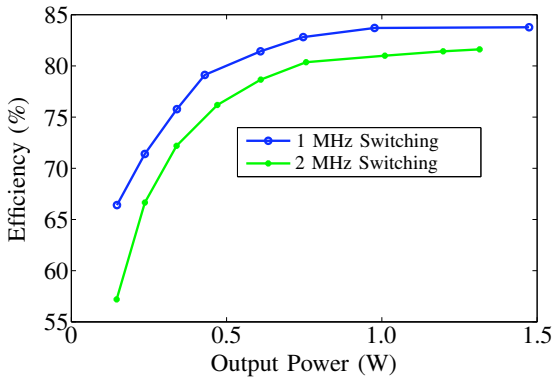

Fig. 11. Miniature power supply efficiency for 1MHz and 2MHz switching frequencies.

The boost converter was implemented on a 25 μm core FR4 custom PC board (like the control board). It was fabricated to match the power connector on the control board and is shown in Fig. 12. Its total weight is 340mg.

C. SMA Drive Method

The boost converter was used as the biasing voltage for an NMOS transistor (FDG6301N). An optional current sensing resistor is routed on the PC board to an A/D input of the PIC processor for closed loop current control (not implemented in this work). The gate of the NMOS was driven by the PIC with a PWM signal (19kHz) to govern the current through the SMA wire. A "spike" plus "normal" current drive method was used to increase efficiency of the actuator. In this method, initial actuation is achieved by a large spike in the current drive that quickly heats the wire. This spike is followed by a lower current level (normal level) that keeps the wire heated. Both actuators were heated in this way. To achieve steering, the two channels were driven with a variable phase difference between them (more on steering in Section V-A).

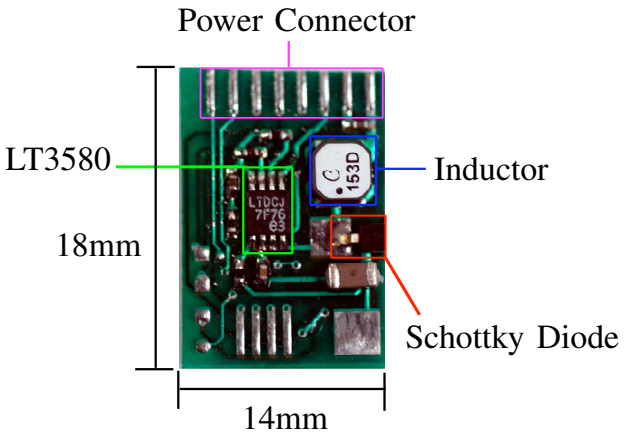

Fig. 12. Miniature boost converter pc board.

D. Communication/Software

As mentioned earlier, the control board utilizes IrDA for wireless communication. Both the gait control PC and the robot control board implement a cyclic redundancy check to detect communication errors. A GUI was written in Matlab to control robot gaits. The software communicates with the robot at all times and can change gaits (if needed) each step cycle. However, the robot is driven in an open loop, teleoperated manner for this work. The step profile is only changed every several steps for turning or stopping.

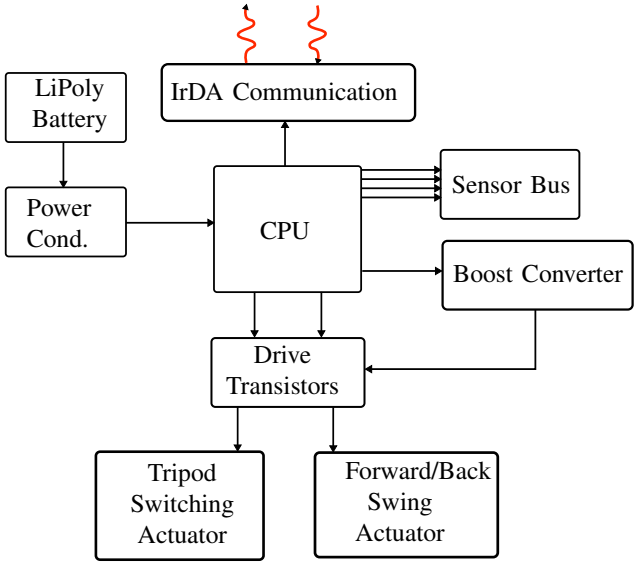

Fig. 13. Electronics block diagram.

V. EXPERIMENTAL RESULTS

The robot was run wirelessly in a series of trials and gait parameters such as the phase delay between the two actuators, current spike duty cycles, and the use of a normal or hold current were tuned experimentally. Our best results show the robot crawling at approximately 1 body length or 3 cm/s. Experimental battery life tests indicate a maximum running time of over 9 minutes when the legs are driven continuously at 3Hz, a frequency just beneath the 3dB point for 37.5 μm SMA wire.

Robot	**Size**	**Mass**	**Onboard Power/Control**	**Speed** (body lengths/sec)
Silicon μbot [4]	1.5cm	83mg	No	0.4
Mesoscale Quadruped [5]	9cm	104g	Yes	3
LIPCA Hexapod [15]	12cm	35g	No	1.5
HexBug [2]	5cm	15.6g	Yes	1.2
RoACH	3cm	2.4g	Yes	1

TABLE IV

A COMPARISON OF SIMILARLY SIZED LEGGED ROBOTS

A. Turning Control

To achieve turning, differential leg lengths were used. Both middle legs are slightly shorter than the four corner legs. During front/back swing actuation, the lateral degree of freedom is actuated before the swing finishes. This momentarily places the four corner legs on the ground simultaneously without the middle legs engaging with the ground. Since the legs on the left side are moving in the opposite direction to the legs on the right, a moment is applied to the robot. Slipping on one or both of the sides will occur, causing the robot to turn. As seen in Fig. 14, both left and right turning can be controlled simply through timing the actuation of the lateral (tripod switching) degree of freedom. In the attached video, we also demonstrate that with zero forward velocity, the robot is capable of turning at a rate of approximately 1.5 rad s^{-1}

VI. DISCUSSION AND FUTURE WORK

We have presented mechanical and electronic designs as well as experimental results for a new autnomous 2.4g hexapedal millirobot called RoACH. The robot is enabled by the SCM process for fabricating articulated composite structures with micron scale features in a nearly monolithic fashion. We have demonstrated straight walking and controlled turning at speeds up to 3 cm/s. To the authors' knowledge, RoACH represents the smallest and lightest autonomous legged robot to date. It is our hope that this demonstration of the viability of the SCM process for designing and fabricating milliscale robots will encourage new developments and novel designs in millirobotic systems.

Future work includes developing a dynamic model of RoACH as well as introducing compliance into the legs and increasing the frequency of operation. The addition of sensors and more complex behavior based on sensory input is also planned.

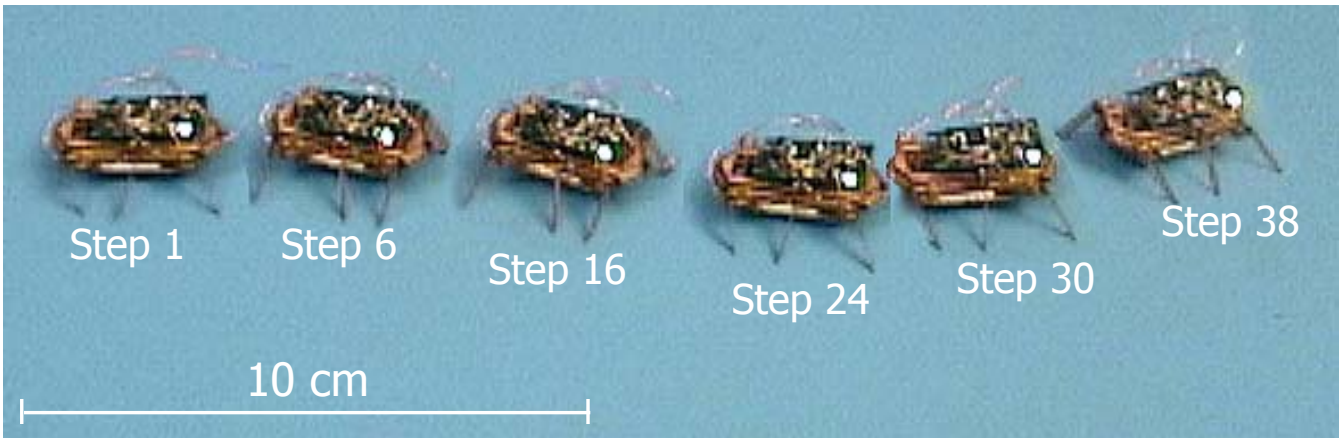

Fig. 14. Composited frame captures from video demonstrating controlled right and left turning

VII. ACKNOWLEDGEMENTS

The authors thank Bryan Schubert for naming RoACH. This work was supported under NSF DMI Grant No. 0423153.

REFERENCES

[1] [Online]. Available: http://dynalloy.com/TechSheets.shtml
[2] [Online]. Available: http://www.hexbug.com
[3] T. J. Dawson and R. C. Taylor, "Energetic cost of locomotion in kangaroos," *Nature*, vol. 246, no. 5431, pp. 313–314, 1973. [Online]. Available: http://dx.doi.org/10.1038/246313a0
[4] T. Ebefors, J. U. Mattsson, E. Kalvesten, and G. Stemme, "A walking silicon micro-robot," in *10th Intl Conf on Solid-State Sensors and Actuators*. IEEE, 1999, pp. 1202–1205.
[5] M. Goldfarb, M. Gogola, G. Fischer, and E. Garcia, "Development of a piezoelectrically-actuated mesoscale robot quadruped," *J. of Micromechatronics*, vol. 1, no. 3, pp. 205–219, July 2001.
[6] L. L. Howell, *Compliant mechanisms*. John Wiley & Sons, 2001.
[7] D. L. Jindrich and R. J. Full, "Dynamic stabilization of rapid hexapedal locomotion," *J Exp Biol*, vol. 205, no. 18, pp. 2803–2823, 2002. [Online]. Available: http://jeb.biologists.org/cgi/content/abstract/205/18/2803
[8] S. Kim, M. Spenko, S. Trujillo, B. Heyneman, V. Mattoli, and M. Cutkosky, "Whole body adhesion: hierarchical, directional and distributed control of adhesive forces for a climbing robot," *Robotics and Automation, 2007 IEEE International Conference on*, pp. 1268–1273, 10-14 April 2007.
[9] B. Lambrecht, A. Horchler, and R. Quinn, "A small, insect-inspired robot that runs and jumps," *Robotics and Automation, 2005. ICRA 2005. Proceedings of the 2005 IEEE International Conference on*, pp. 1240–1245, 18-22 April 2005.
[10] M. H. Raibert, "Legged robots," *Commun. ACM*, vol. 29, no. 6, pp. 499–514, 1986.
[11] U. Saranli, M. Buehler, and D. E. Koditschek, "Rhex: A simple and highly mobile hexapod robot," *The International Journal of Robotics Research*, vol. 20, no. 7, pp. 616–631, 2001.
[12] R. J. Wood, S. Avadhanula, R. Sahai, E. Steltz, and R. S. Fearing, "Microrobot design using fiber reinforced composites," *J. Mech. Design*, vol. To appear, May 2008.
[13] R. J. Wood, E. Steltz, and R. S. Fearing, "Optimal energy density piezoelectric bending actuators," *Sensors and Actuators*, vol. 119, pp. 476–488, 2005.
[14] R. Wood, S. Avadhanula, E. Steltz, M. Seeman, J. Entwistle, A. Bachrach, G. Barrows, S. Sanders, and R. Fearing, "Enabling technologies and subsystem integration for an autonomous palm-sized glider," *IEEE Robotics and Automation Magazine*, vol. 14, pp. 82–91, 2007.
[15] A. Yumaryanto, J. An, and S. Lee, "A cockroach-inspired hexapod robot actuated by lipca," *Robotics, Automation and Mechatronics, 2006 IEEE Conference on*, pp. 1–6, Dec. 2006.